Polymer Journal, Vol. 12, No. 11, pp 809—834 (1980)

Rheo-Optical Studies on the Deformation Mechanism of Semicrystalline Polymers. XII. On the Nature of Alpha and Beta Mechanical Dispersions of High-Density Polyethylene in Relation to the Mechanism of Spherulite Deformation*

Thein KYU,** Masayuki YAMADA,*** Shoji SUEHIRO,**** and Hiromichi KAWAI†

Department of Polymer Chemistry, Faculty of Engineering, Kyoto University, Yoshida, Sakyo-ku, Kyoto 606, Japan.

(Received May 9, 1980)

ABSTRACT: Dynamic birefringence and dynamic X-ray diffraction measurements were carried out from 0.008 to 4.3 Hz at various temperatures from −40 to 100°C and also from 0.05 to 3.2 Hz at various temperatures from −30 to 100°C, respectively, in order to study the nature of α and β mechanical dispersions in spherulitic high-density polyethylene. Three mechanical dispersions analogous to the β, α_1, and α_2 processes were obtained and resolved quantitatively into each component. Two dispersions corresponding to α and β processes were observed in the dynamic birefringence and dynamic crystal orientation studies. These α and β dispersions were interpreted in terms of relative contributions of intralamellar crystal-grain reorientation and lamellar orientation, both of which are associated with the dynamic-tensile deformation of spherulitic crystalline texture. Besides the crystalline contributions, substantial noncrystalline contribution to the α process was seen and is believed to have arisen from the orientation of noncrystalline chains in the crystal-grain boundaries. The noncrystalline contribution to the β process was observed to have a large negative in-phase component and a slightly positive out-of-phase component of the dynamic stress-optical coefficient function. This anomalous behavior is explained in terms of the combined contributions from the orientational and distortional birefringence of interlamellar noncrystalline chains as well as on the basis of negative form birefringence. In the dynamic crystal-lattice deformation studies, two dispersions corresponding to the α_1 and α_2 mechanical dispersions were detected. The former α_1 lattice dispersion is considered to be associated with the α crystal-orientation dispersion, whereas the latter α_2 lattice dispersion is believed to be inherent, arising from incoherent lattice vibrations within crystals in which the intermolecular potential suffers a smearing-out effect.

KEY WORDS Rheo-Optical Properties / High-Density Polyethylene / α and β Mechanical Dispersions / Dynamic Birefringence / Dynamic X-Ray Diffraction /

In contrast to the mechanical relaxation of amorphous polymers, the identification of molecular mechanisms of the mechanical-relaxation processes of semicrystalline polymers met with limited success owing to their complex morphology and the inhomogeneity of their internal structures.[1-3] Consequently, the assignment to the α mechanical relaxation of polyethylene has produced a variety of responses from many investigators.[4-15] The prevalent concept is that the α mechanical relaxation is composed of two components, the α_1 and α_2 processes having activation energies of the orders of 25 and 45 kcal mol^{-1}, respectively.[6,9] The generally accepted assignment to the α_1 process seems to be focussed on the crystal-orientation

* Presented in part at the 28th Annual Meeting of the Society of Polymer Science, Japan, Tokyo, May 27, 1979.

** Present address: *Department of Chemistry, McGill University, Montreal, PQ, Canada, H3A 2K6.*

*** Present address: *Passenger Car Engineering Center, Mitsubishi Motors Corporation, 1 Nakashinkiri Hashime-cho, Okazaki 444, Japan.*

*** Present address: *Polymer Research Institute, University of Massachusetts, Amherst, Mass. 01003, U.S.A.*

† To whom correspondence should be addressed.

relaxation associated with the grain-boundary phenomena,[3,4] while the assignment to the α_2 process must be related to the crystal disordering transition arising from the onset of torsional vibrations of the chain molecules within crystal lattice, *i.e.*, the incoherent lattice vibrations within the crystals in which the intermolecular potential suffers a smearing-out effect.[16,17] The interpretation for the α_2 process may be more or less established as being associated with the development of intracrystalline nonelasticity.[4,14,15,8-21] But no direct evidence has yet been achieved from any dynamic measurements. The interpretation for the α_1 process is, however, still in conflict; *i.e.*, it has usually been accepted as being caused by interlamellar shearing,[4,5,10,11] while some newer experimental evidences are going to support the concept of intralamellar shearing.[12,13]

Strictly speaking, however, all the above assignments are considerably speculative and controversial, thus leading to more direct and convincing investigations by means of rheo-optical techniques. In the previous papers of this series,[22-24] the α mechanical dispersion of a low-density polyethylene was investigated in terms of dynamic birefringence and dynamic X-ray diffraction responses. It was found that the frequency dispersions of the dynamic crystal orientation as well as the dynamic birefringence definitely correspond to the α mechanical dispersion of this material with good agreement between the activation energies of the respective processes all in the order of 25 kcal mol^{-1}. Dynamic amorphous orientation, as seperated on the basis of the two-phase hypothesis of the dynamic birefringence, was found to be almost in-phase with dynamic bulk-strain. Dynamic crystal-lattice compliance was found not to exhibit any frequency dependence. The real component becomes larger in magnitude as temperature increases while the imaginary component remains almost zero regardless of frequency and temperature, suggesting that the crystal-lattice deformation is in-phase with dynamic bulk stress and is likely to be elastic in its dynamic response. It was thus concluded that the α mechanical dispersion of this particular low-density polyethylene is governed mainly by the orientation dispersion of elastic crystal grains, *i.e.*, the grain-boundary relaxation, in association with the following three characteristic responses: (i) the dynamic amorphous orientation being in-phase with dynamic bulk-strain; (ii) the dynamic crystal-lattice deformation being also in-phase with dynamic bulk-stress, and (iii) the dynamic crystal orientation lagging behind the dynamic bulk-strain. These three characteristic responses were analyzed in terms of a dynamic deformation model of spherulitic crystalline texture. In this model, the intralamellar shear, rather than the interlamellar shear, involving rotational orientations of the crystal grains within the lamellae, is considered to be necessary for explaining the grain-boundary relaxation.

Despite the above investigations on the low-density polyethylene, the assignment of the α mechanical dispersion is still felt to be speculative and insufficient to account for the mechanical relaxations of polyethylene due to difficulties arising mostly from its complex spherulitic morphology. This led to successional rheo-optical studies on a row-nucleated high-density polyethylene whose morphology is much simpler than the spherulitic one and well characterized.[25-27] In these studies, two types of distinctive orientation mechanisms of crystals were observed to contribute to the low-temperature α_1 process: *i.e.*, (i) the dynamic orientation of the crystal *a*- and *c*-axis with far less orientation of the crystal *b*-axis which dominates in the machine-direction (MD) specimen; and (ii) the dynamic orientation of the crystal *b*- and *c*-axis with far less orientation of the crystal *a*-axis which dominates in the transverse-direction (TD) specimen. From the lamellar morphology of this particular high-density polyethylene having row-nucleated and highly oriented cylindrites along the MD, the former mechanism must involve rotation of the crystal grains around their crystal *b*-axes in association with lamellar detwisting, and be representative of the mechanism occurring in the equatorial zone of uniaxially deformed spherulites. On the other hand, the latter mechanism must involve rotation of the crystal grains around their crystal *a*-axes in association with lamellar shearing, and be representative for the mechanism occurring in the polar zone of the spherulites. Both rotational-orientation mechanisms of the crystal grains, which are undoubtedly intralamellar shear rather than interlamellar shear, were found to have almost identical activation energies in the order of 25 kcal mol^{-1} and to be comparable to that of the α_1 process. The relative contribution of each rotational-orientation mechanism to the α_1 process

of spherulitic specimen is believed to depend on the perfectness of the spherulitic crystalline texture, *i.e.*, heterogeneity and mechanical anisotropy of the texture.

In addition to the above dynamic crystal-orientation mechanisms, the lamellar bending or splaying apart mechanism, which is a sort of lamellar orientation in association with interlamellar shear and results in a negative form birefringence for the MD specimen, was found to be quite in-phase with the dynamic bulk-stress; *i.e.*, hardly contributing at all to the α process, but probably significant to the β process of this particular material. Furthermore, in contrast to the bulk-crystallized low-density polyethylene, the dynamic crystal-lattice compliance function exhibited a remarkable frequency dispersion, especially for the TD specimen, in that the real component varies very gradually at low temperatures but drastically at elevated temperatures, suggesting the development of intracrystalline viscoelastic nature in the vicinity of the α_2 mechanical dispersion.

In this paper, the rheo-optical properties of a bulk-crystallized high-density polyethylene will be investigated in order to confirm the above assignments to the α_1 and α_2 mechanical dispersions and possibly to the β mechanical dispersion of polyethylene. That is: whether the two types of rotational-orientation dispersions of the crystal grains are really investigated for the spherulitic high-density polyethylene so as to assign the α_1 mechanical dispersion to the intralamellar shearing; the dynamic crystal-lattice compliance function behaves as assigning the α_2 mechanical dispersion to the development of the intracrystalline viscoelasticity; and the β mechanical dispersion is really related to the interlamellar shearing in association with lamellar orientation in the spherulitic texture.

Sample Preparation

Commercial pellets of a high-density polyethylene (Sholex 6009, Japan Olefin Chemical Ind., Ltd.) having a viscosity-average molecular weight of 67,000 and a degree of branching of 0.7 CH_3/1000 carbons were placed in a spacer sandwiched between two polished stainless steel plates, and molten at 180°C in a laboratory hot press for 10 min. A pressure of 200 kg cm^{-2} was applied for another 10 min at the same temperature, and the melt was slowly cooled down to 125°C, and then

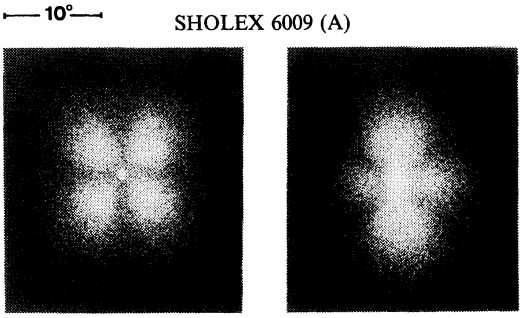

Figure 1. Polarized light-scattering patterns under cross (H_V) and parallel (V_V) polarizations of a high-density polyethylene Sholex 6009 (A).

kept for 2 h at the temperature of 125°C. The stainless plates containing the melt were removed from the press and immediately plunged into ice water to obtain a quenched sample in sheet form. This quenched sample was annealed at 105°C for 4 h in a vacuum oven and gradually cooled down to ambient temperature. The thickness of the sheet specimen was adjusted by the spacer so as to be 60 μm for the dynamic birefringence measurements and 500 μm for the dynamic X-ray diffraction measurements. The annealed specimen is hereafter designated as Sholex 6009 (A). From polarized light-scattering investigations, the annealed specimen was found to have a well-developed spherulitic crystalline texture whose H_v and V_v patterns are shown in Figure 1. Average size of the spherulites was estimated from the H_v pattern to be about 14 μm in radius. The density of the annealed specimen was determined to 0.957 g cm^{-3} by a methanol–water density gradient column at 25.0°C.

Experimental Procedure

The annealed sheet specimen was cut into a ribbon shape of 8 cm long and 8 mm wide for the dynamic mechanical and birefringence measurements. The ribbon-shape specimen was engaged in a tensile dynamic deformation apparatus at an initial gauge length of 6 cm, and was subjected to a static tensile strain of 4.6% superposed with a dynamic tensile strain of 0.32%. A preparatory vibration was applied at 4.3 Hz for one hour to assure the vibrational steady state and to perform a sort of mechanical conditioning of the specimen. Using the π-sector technique,[28] the dynamic mechanical and birefringence measurements were conducted over a

frequency range from 0.008 to 4.3 Hz at various temperatures from −40 to 100°C.

For the dynamic X-ray diffraction measurements, the ribbon-shape specimen 10 cm long and 15 mm wide was engaged with a static tensile strain of 5.0% superposed with a dynamic tensile strain of 0.46%. The preparatory vibration was also applied prior to the dynamic measurements. Applying an improved multichannel narrow sector technique,[29] the dynamic X-ray diffraction measurements were performed over a frequency ranging from 0.05 to 3.2 Hz at various temperatures from −40 to 100°C by scanning twice the Bragg angle from 12 to 28° at a 0.2° interval and the azimuthal angle from 0 to 90° at a 22.5° interval.

The dynamic X-ray diffraction measurements were carried out to investigate the dynamic crystal responses, such as dynamic orientation and dynamic crystal-lattice deformation, as well as the static responses, *i.e.*, the static orientation and lattice deformation caused by the static tensile strain. As has been discussed elsewhere in detail,[29] the dynamic X-ray diffraction intensity, $I=I^0+\Delta I^* e^{i\omega t}$ against the mechanical excitation (dynamic extension ratio) $\lambda=\lambda^0+\Delta\lambda^* e^{i\omega t}$, can be measured as a function of twice the Bragg angle $2\theta_B$ and azimuthal angle ϕ, from which the desired parameters for the dynamic as well as static crystal responses mentioned above can be achieved.

EXPERIMENTAL RESULTS

Static Crystal Responses

Let us first show the static crystal responses obtained from the static X-ray diffraction intensity distribution $I^0(2\theta_B, \phi)$, the details of which procedure are described elsewhere.[25]

Static Crystal Orientation. Figure 2 shows the temperature dependence of static crystal orientation of the annealed specimen under a constant elongation of 5.0%. The degree of crystal orientation is represented in terms of the Hermans orientation factor, *i.e.*, a second-order uniaxial orientation factor defined by $F_k^0=(3\langle\cos^2\theta_k\rangle-1)/2$, where θ_k is the angle between the kth crystallographic axis and the stretch direction, and $\langle\ \rangle$ means the average of its contents. F_a^0, F_b^0, and F_c^0 for the crystal a-, b-, and c-axis, respectively, as well as F_{110}^0 for the reciprocal lattice vectors of the (110) crystal plane are illustrated. As can be seen in the figure, F_c^0 appears to be slightly negative while F_c^0 and F_a^0 appear to be opposite in sign but almost equal in magnitude in the vicinity of about 0.05, all slightly decreasing with increasing temperature. This static crystal orientation behavior can only be explained in terms of uniaxial deformation of spherulites accompanied not only by lamellar orientation, but also by reorientation of crystal grains within the lamellae. As was fully discussed previously,[30-34] the crystal reorientation must occur in two different fashions of preferential rotations of the grains around the crystal b- and a-axis, respectively, at both the equatorial and polar zones of spherulites, so as to orient the crystal c-axis toward the strech direction. Although the lamellar detwisting involving the former rotational mechanism of crystal grains at the equatorial zone may be taken as predominant over the lamellar shearing involving the latter rotational mechanism of crystal grains at the polar zone, these fundamental deformation mechanisms of spherulites must be noted so as to understand the dynamic rheo-optical behavior of polyethylene.

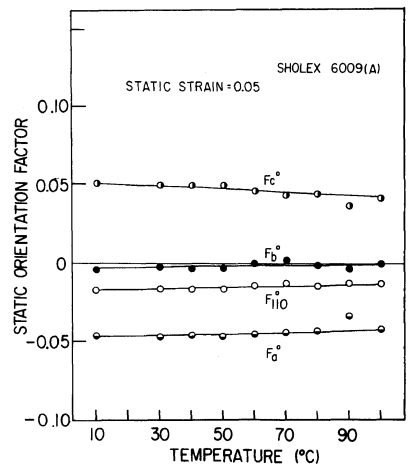

Figure 2. The variation of static-orientation factors of (110) crystal plane and three principal crystallographic axes with temperature.

Static Crystal Lattice Deformation. Figure 3 shows the temperature dependences of the static crystal-lattice spacings of the (110) and (100) crystal planes and of the degree of crystallinity of the specimen, and under a constant elongation of 5.0%. The degree of crystallinity obtained from the static X-ray diffraction intensity distribution is consistent

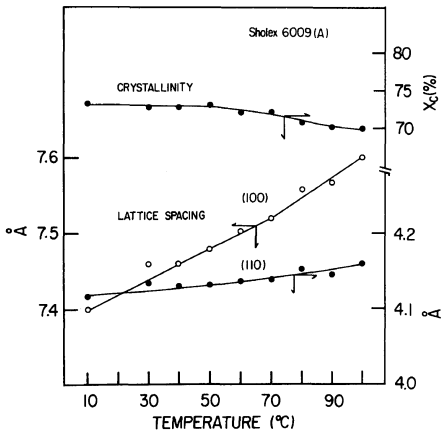

Figure 3. The temperature dependence of the degree of crystallinity and static lattice spacing of the (110) and (100) crystal planes.

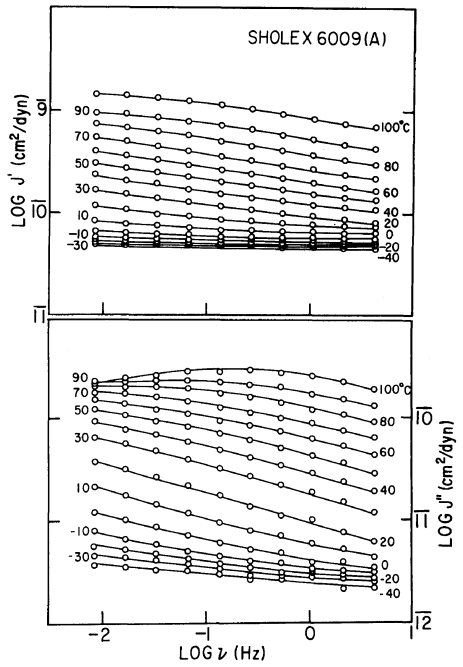

Figure 4. The temperature dependences of storage and loss compliance functions of a high-density polyethylene Sholex 6009 (A).

with that obtained by the methanol-water density gradient column method, showing no appreciable change at low temperatures but gradual decrease at elevated temperatures. The lattice spacings, particularly that of the (100) crystal plane, change their slopes against temperature at around 70°C. This inflection point corresponds to the crystal disordering transition at which the thermal-expansion coefficient of the crystal *a*-axis changes abruptly owing to the onset of rotational vibrations of molecular chains within the lattice.

Mechanical Dispersion

Figure 4 illustrates temperature dependence of the storage and loss compliance functions of the Sholex 6009 (A) specimen. The storage compliance reaches a minimum value of around 4.5×10^{-11} cm^2 dyn^{-1} at the lowest temperature of -40°C, but increases gradually with decreasing frequency at elevated temperatures. The loss compliance increases remarkably with decreasing frequency and exhibits an absorption peak at 100°C. In agreement with the previous studies,[22,27] the conventional frequency-temperature superposition by a simple horizontal shifting of the compliance functions along logarithmic frequency axis is not valid, thus leading to the requirement of a vertical shift in the functions for the purpose of achieving good superposed master curves of the functions.

The application of the vertical shift in conjunction with the horizontal shift in the superposition is usually arbitrary. To minimize the arbitrariness of the procedure, superpositions of the storage and loss compliance functions are performed simultaneously in order that the resulting shift factors give the best possible superposition for both master curves. The superposed master curves for the storage and loss compliance functions reduced to a common reference temperature of 50°C are shown in Figure 5. It can be seen that the frequency dispersion of the loss compliance master curve is unusually broad, suggesting the coexistence of more than a single retardation mechanism contributing to the dispersion.

In Figure 6, the Arrhenius plots in which the logarithm of horizontal-shift factor, log a_T, is plotted against reciprocal of absolute temperature is shown together with the temperature dependence of vertical-shift factor log b_T. The Arrhenius plots can be represented in terms of three distinct straight lines from whose slopes the activation energies of the corresponding retardation processes were estimated to be 18.2, 26.3, and 42.0 kcal mol^{-1}. These values and their corresponding temperature regions suggest that the changing slopes manifest

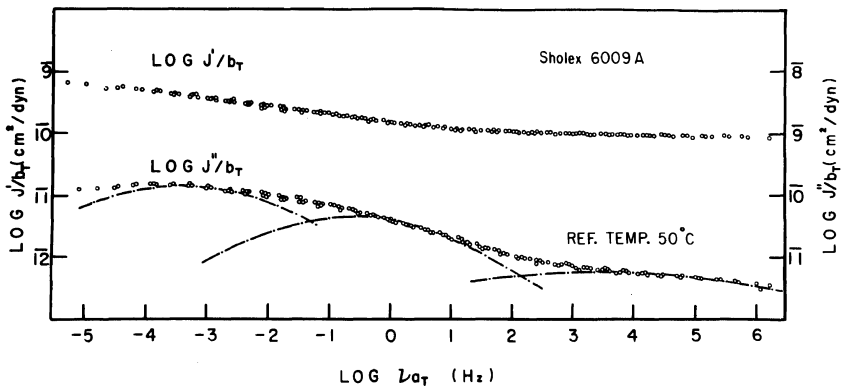

Figure 5. The superposed master curves of storage and loss compliance functions reduced to a reference temperature of 50°C.

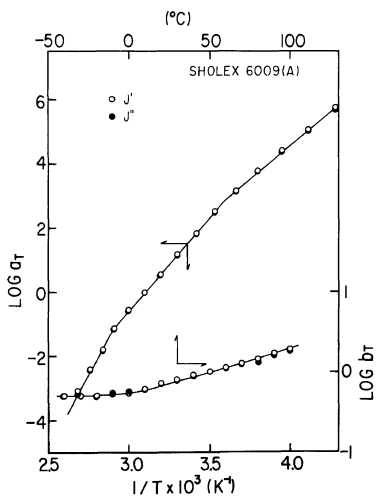

Figure 6. The Arrhenius plots of the horizontal-shift factor log a_T *vs.* reciprocal absolute temperature together with the temperature dependence of vertical-shift factor log b_T.

the β, α_1, and α_2 retardation processes of polyethylene. Knowing that the frequency dispersion in the reduced master curve of loss compliance function is unusually broad and that there appear three linear regions in the Arrhenius plots, one should be able to recognize that the reduced master curve is just "apparent" one, and not unique, since it is not independent of the reference temperature or reduced frequency. These require us to resolve the three retardation mechanisms into constituent contributions to obtain a unique master curve by means of some adequate procedure, such as the procedure proposed by Kawai *et al.*[35,36] In their procedure, the following assumptions were adopted; *i.e.*, (i) additivity for assessing the contribution of each retardation (or relaxation) mechanism to the viscoelastic functions, (ii) validity of the time-temperature superposition hypothesis within each retardation (or relaxation) mechanism independently of the other mechanism, and (iii) the symmetric loss compliance (or modulus) function of each retardation (or relaxation) mechanism with respect to logarithmic time scale.

In accordance with the phenomenological theory based on the above three assumptions, the dynamic storage and loss compliance functions may be formulated in terms of the additivity of the jth retardation mechanisms as follows.

$$J'_T(\omega) = \sum_{j=1}^{m} (\rho/\rho_0) f_j(T, T_0) \sum_{i=1}^{n} J_{j,i}(T_0) \frac{1}{1+\omega^2\tau_{j,i}^2(T_0)a_{T_j}^2}$$

$$= \sum_{j=1}^{m} (\rho/\rho_0) f_j(T,T_0) J'_{j,T_0}(\omega a_{T_j}) \qquad (1)$$

$$J''_T(\omega) = \sum_{j=1}^{m} (\rho/\rho_0) f_j(T, T_0) \sum_{i=1}^{n} J_{j,i}(T_0) \frac{\omega\tau_{j,i}(T_0)a_{T_j}}{1+\omega^2\tau_{j,i}^2(T_0)a_{T_j}^2}$$

$$= \sum_{j=1}^{m} (\rho/\rho_0) f_j(T, T_0) J''_{j,T_0}(\omega a_{T_j}) \qquad (2)$$

where j is the number of retardation mechanisms, and i is the number of retardation elements within the jth retardation mechanism in which the elements have the identical shift factor a_{T_j} and the respective elastic compliances $J_{j,i}$ and retardation times $\tau_{j,i}$.

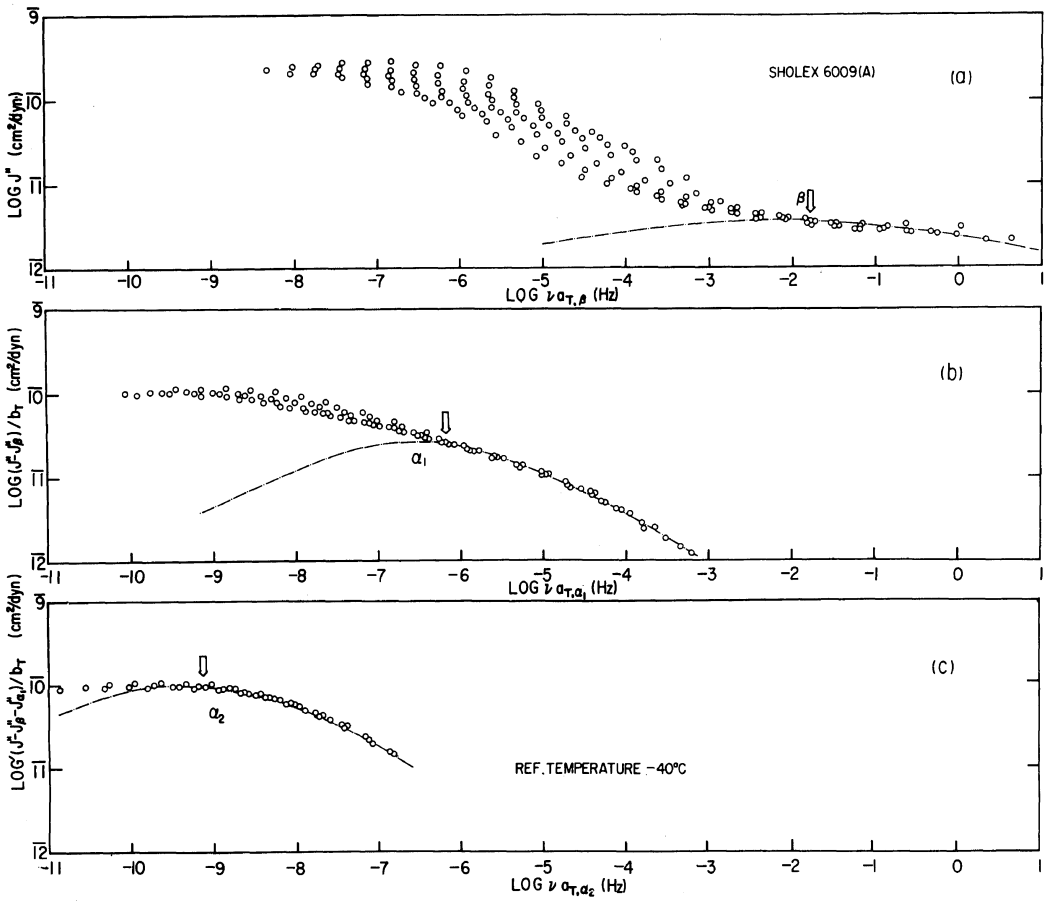

Figure 7. The master curves of loss compliance function superposed in accordance with (a) log $a_{T,\beta}(T, T_0)$ of β process, (b) log $a_{T,\alpha_1}(T, T_0)$ of α_1 process, and (c) log $a_{T,\alpha_2}(T, T_0)$ of α_2 process of Sholex 6009 (A), reduced to a reference temperature of $-40°C$.

$f(T, T_0)$ arises from the identical temperature dependence of the ith elastic compliance $J_i(T)$ within the jth mechanism, and $(\rho/\rho_0)f_j(t, t_0)$ is the correction factor associated with the vertical-shift factor b_{T_j} for the time-temperature superposition for the jth mechanism. The function $f_j(T, T_0)$ is expressed in a general form which varies with the nature of elastic compliance in the jth mechanism; for example, if the jth mechanism has entropic elasticity, the function may be given by (T/T_0).

In addition to the above formulation, a symmetric functional form may be assumed for the frequency dispersion of the loss compliance function of each retardation mechanism as, for instance, a Gaussian-type function with respect to reduced logarithmic frequency, *i.e.*,

$$\log J''_{j,T_0}(\omega a_{T_j}) = (A_j - B_j) \exp\left[-C_j\{\log(\omega a_{T_j}) - \log(\omega a_{T_j})_0\}^2\right] + B_j \quad (3)$$

where $A_j (= \log J''_{j,\max})$ is the maximum loss compliance, $B_j (= \log J''_{j,\min})$ is the asymptotic minimum loss compliance being practically able to assume as negligibly small, $(\omega a_{T_j})_0$ is the reduced frequency at which the maximum loss compliance appears, and C_j is the parameter characterizing the broadness of the jth mechanical dispersion.

In Figure 7(a) is shown the superposed master curve of the loss compliance function reduced to a reference temperature of $-40°C$ by shifting the original loss compliance data in Figure 4 horizontally along the logarithmic frequency axis without necessitating any vertical shift in accordance with

the shift factor $a_{T,\beta}(T, T_0)$ of the low temperature β process up to higher temperatures as shown in Figure 9. The Arrhenius plots are thus represented by a single straight line extrapolated to high temperatures. Such superposition has to be carried out on the assumption that there exists only one mechanism which follows the Arrhenius-type retardation process, so that any deviation from the master curve may be attributed to additional retardation mechanisms. It is evident that only the higher reduced frequency portion of the master curve superposes pretty well with a somewhat broad absorption peak, as indicated by an open arrow whereas the lower frequency data scatter substantially and are poorly superposed. This suggests the existence of additional retardation processes at high temperatures.

Three parameters, *i.e.*, peak position, magnitude, and broadness, have been required for characterizing the broad β dispersion in terms of a symmetric Gaussian-type function. The peak position and magnitude of the superposed portion corresponding to the β dispersion can be determined, within the limit of experimental error, by adjusting the broadness parameter so that the resulting Gaussian-type function gives the best possible fit. Since the magnitude of the loss compliance at low-temperature or high-frequency portion nearly comes to being smaller by an order of about two decades than those of high temperatures, the arbitrariness that might involve in the resolution is perhaps not significant.

The residual data of the loss compliance after separating the β process are shown in Figure 8(b). As with the superposition of the original data, the residual data are re-superposed with a different horizontal-shift factor, $a_{T,\alpha_1}(T, T_0)$, required for the α_1 process by referring the same reference temperature of -40°C as depicted in Figure 7(b). At this time, the vertical shift is required for obtaining a good superposed master curve. It is obvious from Figure 7(b) that the high-frequency portion of the master curve superposes very well with a somewhat broad absorption peak as indicated by an open arrow. But there appear again poorly superposed data that considerably deviate from the master curve, suggesting that additional dispersion mechanism other than the α_1 process still exists at lower reduced-frequency portion. The α_1 mechanical dispersion can be characterized by a Gaussian-type function by adjusting its parameters. Since the vertical shift is needed for the superposition, the determination of the parameters of Gaussian-type function and the vertical-shift factor produces some arbitrariness. To minimize this arbitrariness, the determination is conducted by means of a trial and error method so that the resolved data for the higher-temperature process do not necessitate any further vertical translation in the subsequent superposition.

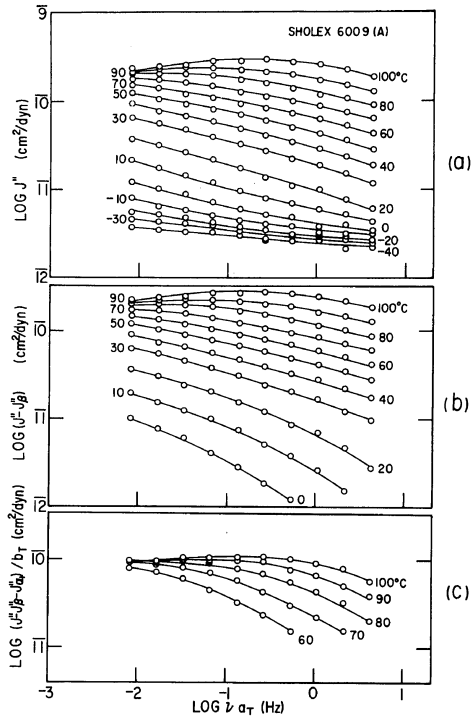

Figure 8. The temperature and frequency dependences of (a) original loss compliance function, (b) residual loss compliance function after separating the β process, and (c) residual loss compliance function after separating the β and α_1 process of Sholex 6009 (A).

The resolved data of the loss compliance after separating the β and α_1 dispersions are illustrated in Figure 8(c). It is evident that the maximum values of the loss compliance functions are nearly equal, implying that no vertical shift would be further required in the subsequent superposition of the higher-temperature process. Figure 7(c) shows the superposed master curve obtained by shifting the data in Figure 8(c) horizontally in accordance with the horizontal-shift factor of $a_{T,\alpha_2}(T, T_0)$, reduced to

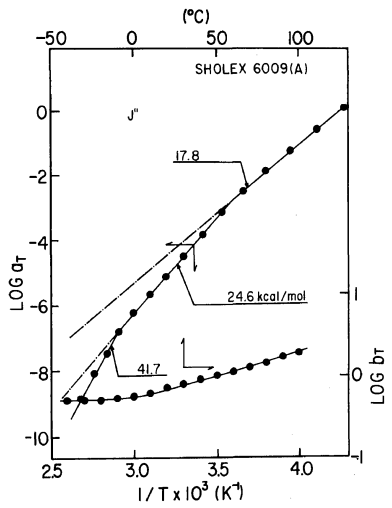

Figure 9. The Arrhenius plots of the horizontal-shift factor log a_T *vs.* reciprocal absolute temperature together with the temperature dependence of vertical-shift factor log b_T of Sholex 6009 (A) referring -40°C as the reference temperature.

the same reference temperature of -40°C. The absorption peak is obvious and can be characterized by a Gaussian-type function for the α_2 process. Yet, some deviation can be noted at the lowest frequencies which are perhaps associated with the further additional retardation process related to the premelting of crystal or plastic flow of the system at such high temperatures.

The temperature dependences of the horizontal- and vertical-shift factors, $a_{T,j}(T, T_0)$ and $b_{T,j}(T, T_0)$, thus determined are plotted in Figure 9. Comparing these with the plots for the apparent superposition in Figure 4, the temperature dependences of $a_{T,j}$ are found to be slightly modified, having the activation energies of the respective processes of 17.8, 24.6, and 41.7 kcal mol^{-1}, whereas those of $b_{T,j}(T, T_0)$ are hardly changed. The temperature dependence of the vertical-shift factor is not appreciable at low temperatures, but becomes severe with ascending temperature. The significance of this severe temperature dependence will be discussed later in connection with that of the vertical-shift factor of the dynamic crystal-lattice compliance function.

The resolved loss compliance dispersions are displayed together in Figure 5 by dash-dot lines, using the temperature dependences of $a_{T,j}$ and $b_{T,j}$ in Figure 9 to adjust the reference temperature from -40 to 50°C. The resolved and unresolved (apparent) master curves are in fairly good agreement, indicating definitely that the broad loss compliance function contains three mechanical dispersions corresponding to the β, α_1, and α_2 retardation mechanisms.

Dynamic Crystal Responses

Let us show the dynamic crystal responses obtained from $\Delta I^*(2\theta_B, \phi)$. The improved multichannel-narrow-sector technique of dynamic X-ray diffraction[29] permits the simultaneous investigation of dynamic crystal orientation and dynamic crystal-lattice deformation.

Dynamic Crystal Orientation Dispersion. The dynamic crystal-orientation behavior is analyzed in terms of the complex dynamic stress-orientation coefficient function, $D^*_k(=D'_k - iD''_k)$, which is defined as the derivative of complex dynamic amplitude of the second-order orientation factor of the k th crystallographic axis with respect to that of bulk stress. That is, $D^*_k(i\omega) \equiv (\partial F^*_k/\partial \sigma^*)|_{\sigma=\sigma^0}$, where F_k is the Hermans uniaxial-orientation factor. In Figures 10 and 11 are shown the frequency dispersions of the real and imaginary components of D^*_k, respectively, over a temperature range from -30 to 100°C for reciprocal lattice vector of the (110) crystal plane and three principal crystallographic axes, a-, b- and c-axis. D^*_b and D^*_c are calculated from the experimental data of D^*_{110} and D^*_{200} based on a relationship between F_k proposed by Wilchinsky.[37]

The negative sign of D^*_k implies that the k th crystal axis orients away from the stretching direction. The temperature and frequency ranges of the dynamic X-ray diffraction measurements cover the α_1 and α_2 mechanical dispersion regions and possibly a part of the β mechanical dispersion region. As can be seen in the figures, there is the possibility of D'_k and D''_k becoming opposite in sign to each other at low temperatures, though the accuracy of the measurement of D''_k, especially when it takes on an extremely small value near zero, is not high enough to distinguish it as being positive or negative. At relatively moderate temperatures, it is noted that the D'_b attains a maximum with a positive sign while D'_a is negative in sign and D'_c is very close to zero but still definitely negative in sign. At relatively high temperatures, on the other hand, the D'_c reverses its sign from negative to positive but the

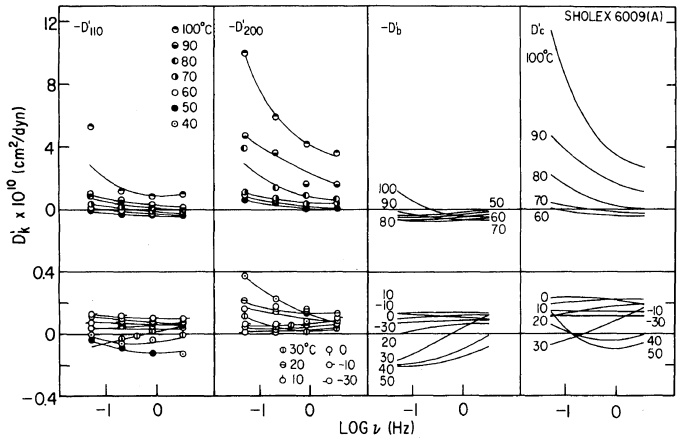

Figure 10. The variation of the real component of stress-optical coefficients D'_k of the (110) crystal plane and crystal *a*-, *b*-, and *c*-axes with frequency in high- and low-temperature regions.

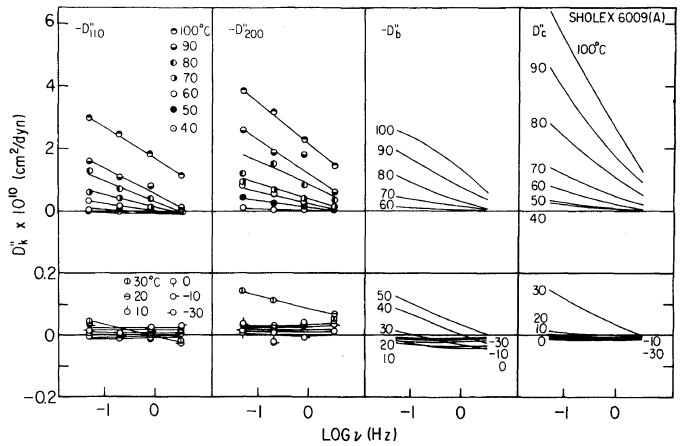

Figure 11. The variation in the imaginary component of stress-optical coefficients D''_k of the (110) crystal plane and crystal *a*-, *b*-, and *c*-axes with respect to frequency in high- and low-temperature regions.

D'_a still remains negative, then both vary drastically with frequency in contrast to the rather lenient dispersion of D'_c.

The variations of real and imaginary components of D_k^* are so drastic that their magnitudes decrease more than one decade as the frequency increases or the temperature decreases. In fact, it is best to plot D_k^* on a logarithmic scale, but since the D_k^* undergoes a change in sign from negative to positive or *vice versa* depending on the k th axis, a plot on a logarithmic scale is not possible unless this problem of sign reversal is solved in terms of the superposition of different orientation mechanisms, as will be discussed later.

In contrast to the strain-orientation coefficient function C_k^*,[22,38,39] a conventional frequency-temperature superposition only by horizontal shift of the original data along logarithmic frequency axis by an amount of $\log c_T$ is not valid, thus requiring a considerable amount of vertical shift in D_k^* by the factor z_T. Master curves of the real and imaginary components of D_k^* thus composed and reduced to a reference temperature of 50°C are shown in Figure 12. The original data at the lowest temperatures of -20 and -30°C are omitted due to the scattering of D''_k near zero and to difficulty of distinguishing D''_k

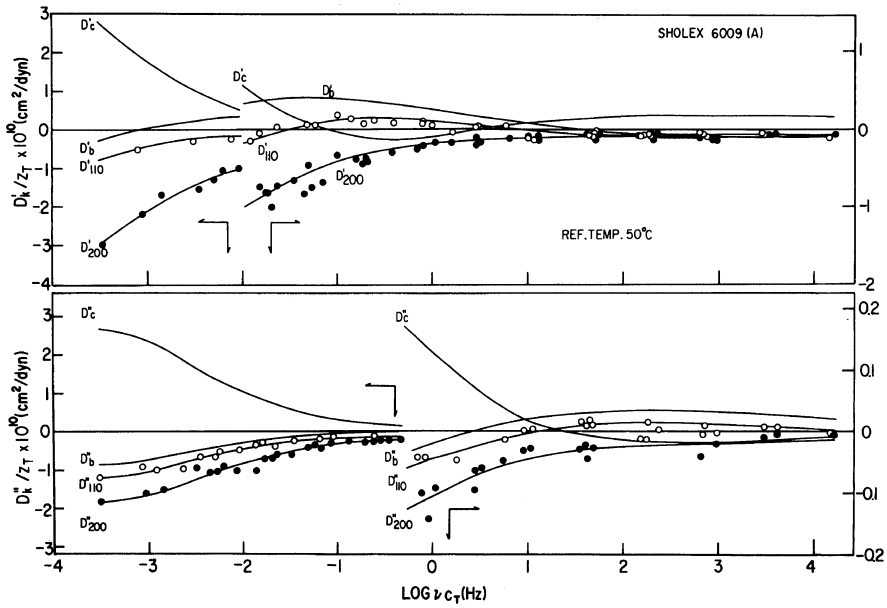

Figure 12. The superposed master curve of the real and imaginary components, D'_k and D''_k, of the complex dynamic stress-orientation coefficient function for the (110) and (200) crystal planes and crystal *b*- and *c*-axes reduced to a reference temperature of 50°C.

to be positive or negative. Although the master curves are again the 'apparent' ones in the sense that the system has different orientation-retardation mechanisms, as suggested above, the following anomalies in the dynamic-orientation behavior must be noted: D'_k and D''_k becoming opposite in sign as observed for D_b^* and D_c^* at relatively high reduced frequencies, for D_c^* at moderate frequencies, and for D_b^* at low frequencies; D'_b and D''_c exhibiting a distinctive positive maximum and a slight negative minimum, respectively, at moderate frequencies, not of leveling off but of a change in sign with further decreasing frequency. None of these anomalies can be explained in terms of a single orientation-retardation mechanism of crystal, but by the superposition of at least two different orientation mechanism in the crystalline phase.

As a matter of fact, the temperature dependence of the horizontal-shift factor $c_T(T, T_0)$ can be represented by two straight lines bent at around 15°C in their Arrhenius plots, as shown in Figure 13. The activation energies of the respective orientation-retardation processes are estimated as 24.4 and 19.9 kcal mol^{-1}. These values and their corresponding temperature regions suggest the

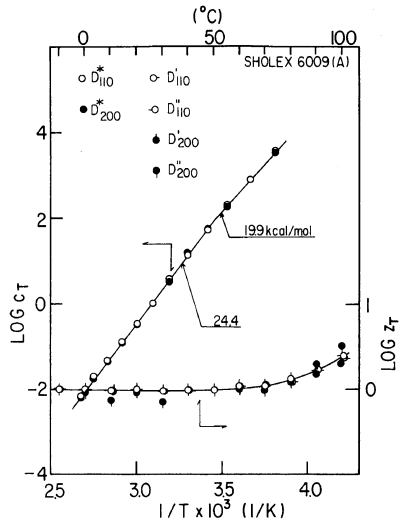

Figure 13. The Arrhenius plots of horizontal-shift factor log c_T *vs.* reciprocal absolute temperature together with the temperature dependence of vertical-shift factor log z_T that are required in the superposition of complex dynamic stress-orientation coefficient functions.

occurrence of α and β orientation dispersions. It is noteworthy that these activation energies are in good agreement with those of the α_1 and β mechanical dispersions. The interesting fact is that no dispersion corresponding to the mechanical α_2 dispersion is observed. Judging from their activation energies and the temperature regions, the β orientation dispersion does correspond to the β mechanical dispersion, while the α orientation dispersion corresponds only to the α_1 mechanical dispersion.

The change in the dynamic crystal-orientation behavior from a slightly positive b-axis orientation in D'_b at moderate frequencies to a very positive c-axis orientation in D'_c at low frequencies, must be explained at least qualitatively in terms of the increasing contribution of the crystal-reorientation mechanism (α orientation dispersion process) within crystal lamellae to the lamellar-orientation mechanism (β orientation dispersion process) associated with the dynamic uniaxial deformation of the spherulitic crystalline texture. At relatively low frequencies, it is also noted that the orientation dispersions of D_c^* and D_a^* are much pronounced in contrast to the rather lenient dispersion of D_b^*. This contrast in behavior suggests that the crystal reorientation must occur in the following two preferential fashions; *i.e.*, the rotations of the crystal grains around the crystal b- and a-axes, respectively, associated with the lamellar detwisting and lamellar shearing mostly at the equatorial and polar zones of the deformed spherulites. These crystal reorientations associated with the lamellar detwisting and lamellar shearing have been investigated separately in the MD and TD specimens of a row-nucleated high-density polyethylene to contribute definitely to the mechanical α_1 and optical α dispersions of the specimens.[25-27] More recently, these crystal-reorientation processes have been investigated also explicitly for a spherulitic specimen of the Sholex 6009 (A) in regard to the complex dynamic change in the orientation-distribution function of the crystal grain itself, $\Delta W^*(\theta, \phi, \eta)$.[40] It was confirmed that the crystal rotation around the crystal b-axis must dominate in the equatorial zone of spherulites and predominate over that around the crystal a-axis in the polar zone of the spherulites in the case of this bulk-crystallized specimen.

It may be plausible to analyze the apparent master curves of D_k^* in Figure 12 quantitatively in terms of the contributions of different orientation-retardation mechanisms, at least the α and β retardation mechanisms, by formulating the similar equations as eq 1 and 2 based on the three assumptioms. The equations may be formulated as follows.

$$D'_{k,T}(\omega) = \sum_{j=\alpha}^{\beta} z_{T_j}(T, T_0)\left[D'_{k,j}(\infty) + \int_{-\infty}^{\infty} D_{k,j}(ln\tau)/\{1+\omega^2\tau_j^2(T_0)c_{T_j}^2\}\, d ln\tau \right] = \sum_{j=\alpha}^{\beta} z_{T_j}(T,T_0) D'_{k,j,T_0}(\omega c_{T_j}) \quad (3)$$

$$D''_{k,T}(\omega) = \sum_{j=\alpha}^{\beta} z_{T_j}(T, T_0)\left[\int_{-\infty}^{\infty} D_{k,j}(ln\tau)\omega\tau_j(T_0)c_{T_j} \Big/ \left\{1+\omega^2\tau_j^2(T_0)c_{T_j}^2\right\} d l\eta\tau \right] = \sum_{j=\alpha}^{\beta} z_{T_j}(T, T_0) D''_{k,j,T_0}(\omega c_{T_j}) \quad (4)$$

where $D_{k,j}(ln\tau)$ is the orientation-retardation time spectrum of the kth crystal plane for the jth orientation-retardation mechanism.[24]

The quantitative analyses of the crystal-reorientation (α) and lamellar-orientation (β) mechanisms on the basis of eq 3 and 4 are, however, too arbitrary to be carried out mainly because of the lack of accuracy in original data at low temperatures in Figures 10 and 11 and, consequently, at high reduced frequencies in Figure 12 and partly because of the lack of original data at high temperatures and low reduced frequencies at which D''_k should attain maximum and D'_k tend to level off with further increasing temperature of decreasing frequency. Therefore, only qualitative analyses of D_k^* based on the concept of eq 3 and 4 are schematized in Figure 14 not only to determine the α and β orientation dispersions in the $D^*_{k,jT_0}(\omega c_{T_j})$ but also to explain the anomalies in the dynamic-orientation behavior mentioned above. The schemes at higher reduced frequencies than the frequency indicated by an arrow are, however, simply speculative and are not based on the experimental results.

At low temperatures of high reduced frequencies, the crystal grains within the lamellae may be frozen, causing the lamellae to respond as a rigid body

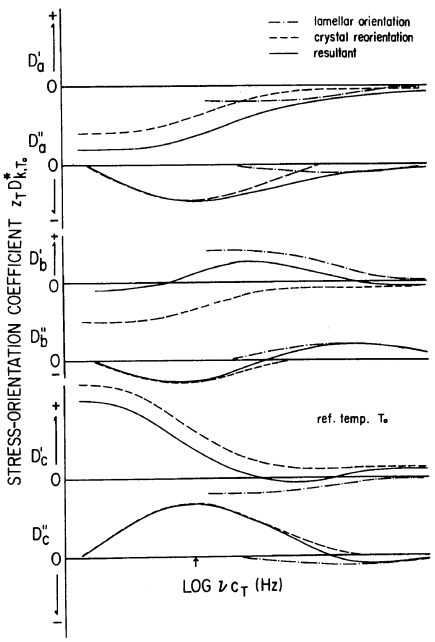

Figure 14. The schematized diagram of the frequency-dispersion behavior of the superposed master curves of the complex dynamic stress-orientation coefficients D_k^* for the three principal crystallographic axes of a high-density polyethylene.

during spherulite deformation since the interlamellar non-crystalline material is activated by the low temperature β process. If the lamellar orientation dispersion were to occur solely in this region, the D_b^* would of course be positive since the crystal b-axis is aligned toward the stretching direction. Consequently, D_a^* and D_c^* are negative. Inasmuch as the D_k^* is always retardational in its dispersion behavior, the D_b' must increase and level off with an decrease in frequency at a rate corresponding to the increase in temperature; the D_c'' however shows a maximum analogous to the frequency region of the transition of D_b'. The negative D_a^* and D_c^* must also behave in retardational manner probably to the same extent, so that the retardation intensity of the crystal a- and c-axis orientation is half of that of the b-axis orientation.

When the temperature increases or frequency decreases, the crystal grains within the lamellae may be activated by the high-temperature α process, resulting in the c-axis orientation associated with reorientation of the crystal grains around the crystal b- or a-axis. This leads to the positive D_c^* dispersion. As a consequence, the D_a^* and D_b^* are negative, but their retardation intensities may be different depending on the relative contribution of the crystal rotation around the crystal b-axis and a-axis. The combination of the crystal-reorientation dispersion with the lamellar-orientation dispersion mentioned above should bring about a result which certainly resembles the dynamic-orientation behavior of the three principal crystallographic axes in Figure 12.

The dynamic crystal-orientation behavior of this bulk-crystallized high-density polyethylene is significantly different from that of a low-density polyethylene.[22] For the high-density polyethylene, the behavior at low reduced frequencies corresponding to the α dispersion region is dominated in terms of the rotation of the crystal grains around the crystal b-axis in association with the lamellar detwisting mostly concentrated at the equatorial zone of spherulites. For the low-density polyethylene, the behavior is quite the opposite, being dominated by the rotation of the grains around the crystal a-axis in association with lamellar shearing concentrated at the polar zone of spherulites. This difference is believed to be reflected by the differences in the perfectness of crystal lamellae constituting the spherulites and in the properties of constituent noncrystalline materials between the lamellae. The crystal lamellae may be of a more paracrystalline nature, greater in mechanical compliance, and less packed within the spherulite for the low-density polyethylene than for the high-density polyethylene. This allows for a more homogeneous deformation of spherulites of low-density polyethylene associated with rather dominant rotation of the crystal grains around the crystal a-axis than around the crystal b-axis.

Dynamic Crystal-Lattice Deformation. The dynamic crystal-lattice deformation obtained simultaneously with the dynamic crystal orientation is analyzed in terms of the apparent dynamic crystal-lattice compliance function $J_k^*(=J_k'-iJ_k'')$ in a sense that this function is defined as the derivative of the complex dynamic amplitude of the tensile-lattice strain of the k th crystal plane with respect to that of bulk stress on assuming that the internal-lattice stress to be identical with the bulk stress. In Figure 15, the real and imaginary components of $J_k^*=J_k'-iJ_k''$, are plotted for the (110) and (200) crystal planes against the azimuthal angle ϕ, in

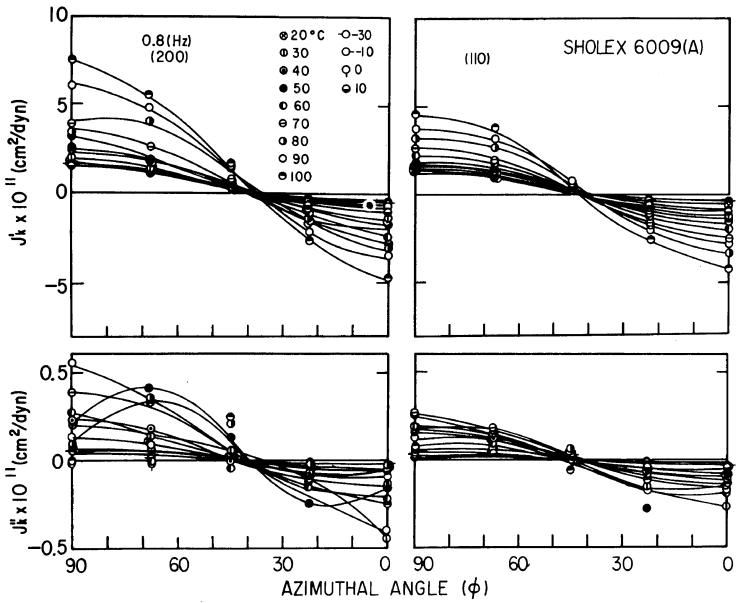

Figure 15. The variations in the real and imaginary components of apparent crystal-lattice compliance J_k^* for the (110) and (200) crystal plane with respect to azimuthal angle ϕ.

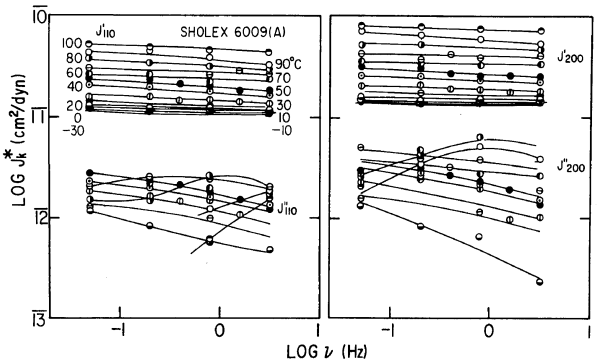

Figure 16. The frequency dispersions of the real and imaginary components of apparent dynamic crystal-lattice compliance J_k^* for the (110) and (200) crystal planes at an azimuthal angle ϕ of 90 for various temperatures.

which the direction of applied stress is normal to the crystal plane under investigation at $\phi=90°$, and is parallel at $\phi=0°$. Contrary to the results for the low-density polyethylene,[22] the J_k'' have appreciable values at either $\phi=90$ or 0°, suggesting that the crystal-lattice deformation is no longer in-phase with the bulk stress and possibly the crystal is very likely to be viscoelastic, rather than elastic, in its mechanical response, though the assumption by which the internal-lattice stress is identified with the bulk stress, *i.e.*, the homogeneous-stress hypothesis, is problematical. The J_k' as well as the J_k'' vary from positive to negative as the azimuthal angle decreases. The positive J_k^* at $\phi=90°$ implies that the crystal lattices are deformed in an extensional manner, while the negative J_k^* at $\phi=0°$ indicates the lattices to be deformed in compressional manner. The same sign for J_k' and J_k'' means that the lattice-

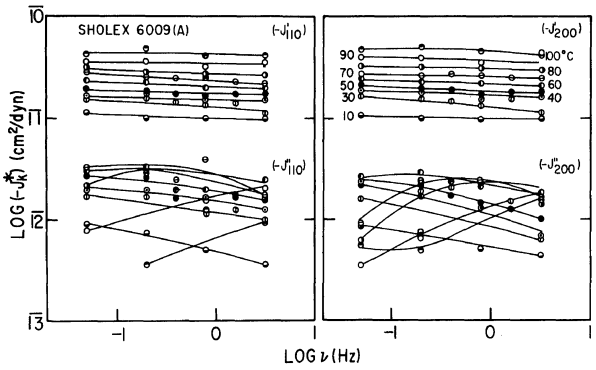

Figure 17. The frequency dispersions of the real and imaginary components of apparent dynamic crystal-lattice compliance J_k^* for the (110) and (200) crystal planes at an azimuthal angle ϕ of 0 for various temperatures.

deformation lags behind the applied stress.

Figure 16 shows the frequency dependences of J_k' and J_k'' at $\phi=90°$ as a function of temperature. As can be seen from the figure, J_k' for the (110) and (200) crystal planes decrease, as the frequency increases and the temperature decreases, and seem to converge to certain values. On the other hand, J_k'' exhibit absorption peaks in the temperature range of 60 to 80°C and still have appreciable values at low temperatures below 50°C, though scattered considerably. At temperatures lower than 10°C, J_k'' take on extremely small values and are scattered too much to distinguish them as either positive or negative, thus these data are omitted in the figure.

Judging from the optical geometry of the dynamic X-ray diffraction measurements, J_{200}^* and J_{110}^* at $\phi=90°$ cause the crystal-lattice deformation behavior at particular zones of uniaxially deformed spherulites with polar angles of 90° (equatorial zone) and 35°, respectively, whereas J_{200}^* and J_{110}^* at $\phi=0°$ yield the behavior averaged over the zones, mentioned above, but not with the particular polar angles with respect to the altered stretching direction. The behavior at $\phi=0°$ is shown in Figure 17, and is very similar to the behavior in Figure 16, irrespective of difference in location of the observed crystal responses within the spherulites. The same sign of J_k^*, though both are negative, implies that the dynamic lattice deformation lags behind the applied stress. $-J_k'$ decreases as the frequency increases and temperature decreases, while $-J_k''$ reveals maximum peaks at intermediate temperatures between 60 and 80°C.

Neither is a conventional frequency-temperature superposition made simply by shifting the data horizontally along the logarithmic frequency applicable in both J_k^* at the azimuthal angles of 0 and 90°, so that considerable amount of vertical shift of the original data along log J_k^* axis is necessary. The master curves reduced to a reference temperature of 50°C for $\phi=90$ and 0° are shown in Figures 18 and 19, respectively. It is seen that the absorption peak of the imaginary components J_k'' for both (110) and (200) crystal planes is very broad at both $\phi=90$ and 0°, and appears in the same reduced frequency range. This is a slight indication that the broad absorption peak is a twin.

The Arrhenius plots of the horizontal-shift factors e_T consists of two straight lines from which the activation energies are estimated to be of the orders of 26 and 42 kcal mol^{-1}, as illustrated in Figure 20. The magnitudes of the activation energies and the corresponding temperature regions certainly correspond to those of the α_1 and α_2 mechanical dispersions. The result of the observance of α_2 process in the dynamic crystal-lattice compliance function was as expected since the crystal-lattice dispersion is directly associated with an intracrystalline nature. The observance of α_1 process in the J_k^* is, however, contradictory to our previous predictions for the low-density polyethylene[22] and row-nucleated high-density polyethylene[25] for which the α_1 process has been accepted as the intercrystalline grain-boundary relaxation phenomenon. This contradiction must be explained in connection with the α crystal orientation dispersion

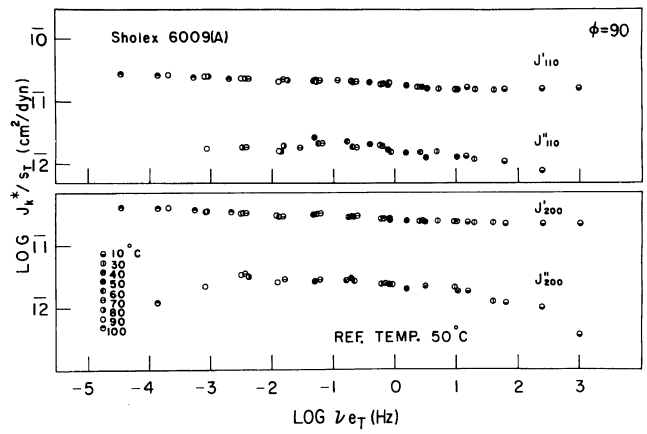

Figure 18. The superposed master curves of the real and imaginary components of apparent dynamic crystal-lattice compliance function for the (110) and (200) crystal planes at $\phi=90°$ reduced to a reference temperature of 50°C.

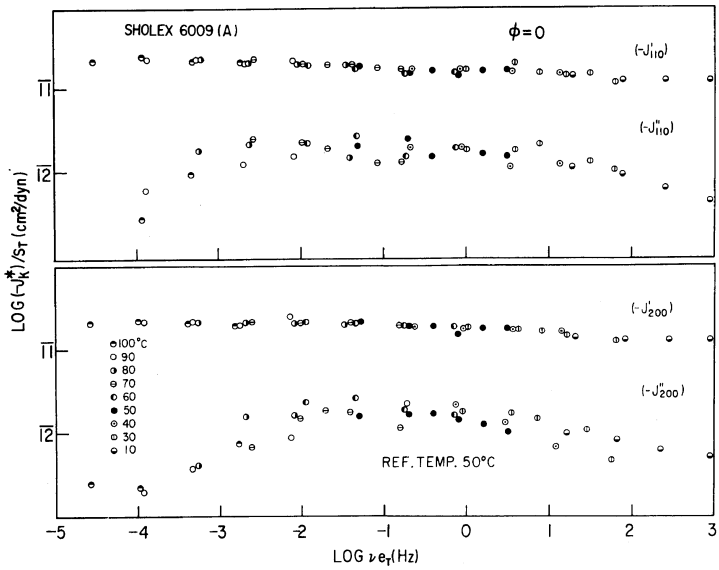

Figure 19. The superposed master curves of the real and imaginary components of apparent complex dynamic crystal-lattice compliance function for the (110) and (200) crystal planes at $\phi=0°$; reduced to a reference temperature of 50°C.

by taking into account the morphological and topological differences in crystalline texture between the specimens.

It is already known that the crystal-reorientation dispersion occurs with an activation energy of the order of 25 kcal mol^{-1} in the vicinity of the α_1 mechanical dispersion. Due to the presence of the large fraction of crystalline component in the high-density polyethylene, the interaction between the crystal grains must be of great importance to account for the correlation of the crystal-orientation dispersion and the crystal-lattice dispersion. The stronger the interaction between the crystal grains, the greater is the coherence of the crystal-lattice

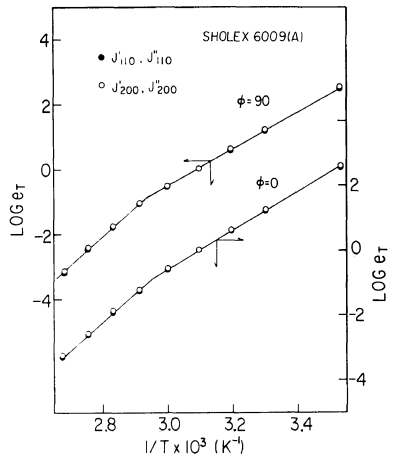

Figure 20. The Arrhenius plots of the horizontal-shift factors log e_T *vs.* reciprocal absolute temperature for both azimuthal angles of 90 and 0°.

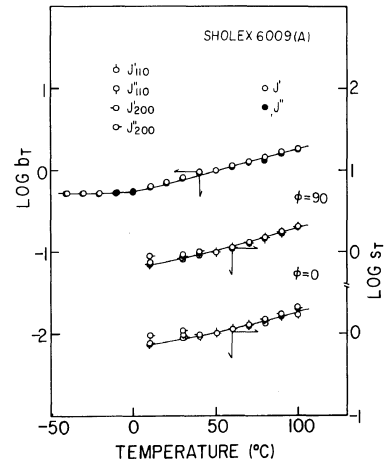

Figure 21. The temperature dependence of the vertical-shift factors log s_T in comparison with that of bulk specimen, log b_T.

dispersion reflecting the crystal-orientation dispersion, even though the crystal grains may be primarily elastic in nature in the time scale region corresponding to the α_1 mechanical dispersion. But in the case of low-density polyethylene, the situation is the otherway around, leading to the fact that the crystal-lattice deformation may not be associated with the α crystal orientation process.

In the vicinity of the α_2 mechanical dispersion, the dynamic crystal-orientation dispersion continues to occur. But the activation energy required to bring about the crystal-orientation dispersion is of the order of 26 kcal mol^{-1} even at high temperatures. To absorb a sizable amount of extra energy, an additional mechanism other than the crystal-orientation dispersion must take place in this time scale region. Hence, the observation of α_2 process in the crystal-lattice dispersion with activation energy of the order of 42 kcal mol^{-1} is believed to be independent of the crystal-orientation process and should be the inherent process arising from the onset of rotational vibrations of chain molecules within the crystal to smear out the elastic potential within the crystal lattice; *i.e.*, the transition of polymer crystal from elastic to viscoelastic in its dynamic response.

The vertical-shift factors required in the superposition of J^*_{110} and J^*_{200} at the azimuthal angles of 0 and 90° are plotted as function of temperature in Figure 21 together with that of the J^* of bulk specimen. It is evident that the temperature dependences of these vertical-shift factors conform very well with that of the bulk specimen. This fact strongly suggests that the requirement of a vertical shift in the superposition of bulk compliance has arisen from the result of the temperature dependence of the crystal-lattice compliance. This accords well with our previous prediction[22,23] that the vertical-shift factors of the elastic modulus function E^* are probably inherent in the temperature dependence of the crystal-lattice modulus E^*_k.

Optical Dispersion

Dynamic birefringence data obtained along with the dynamic mechanical data are analyzed in terms of the real and imaginary components of the complex dynamic stress-optical coefficient function $M^*(=M'-iM'')$. This function is defined as the derivative of the complex dynamic amplitude of birefringence with respect to that of bulk stress. The real component M' is plotted as a function of temperature in Figure 22 by separating the component into high and low-temperature regions. As can be seen in Figure 22, the M' shows a remarkable frequency dispersion at high temperatures and decreases in its magnitude with decreasing temperature in association with the frequency dispersion becoming more lenient at low temperatures. In good agreement with the appearance of the negative real component K' of a high-density polyethylene,[41] the

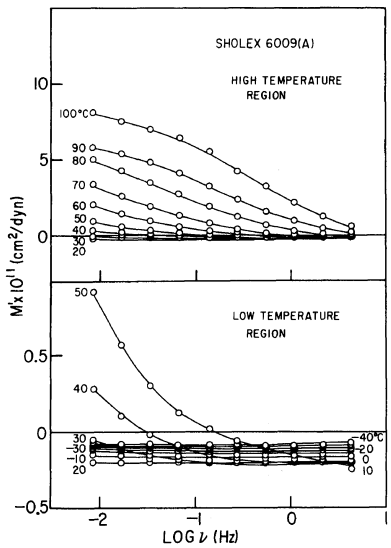

Figure 22. The variation in the real component M' of the complex dynamic stress-optical coefficient function with frequency in high- and low-temperature regions.

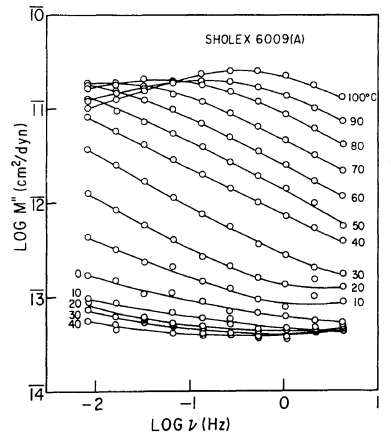

Figure 23. The variation in the imaginary component M'' of the complex dynamic stress-optical coefficient function with frequency at various temperatures.

M' does become negative at low temperatures, attaining a maximum in its negative magnitude at around 20°C and varying very slightly with frequency.

In Figure 23, the imaginary component M'' is plotted in its logarithmic scale against logarithmic frequency. It is seen that the M'' also shows a definite frequency dispersion corresponding to that of the M', exhibiting a distinct frequency dispersion peak at high temperatures of around 100°C and an additional very lenient dispersion associated even with a slight minimum in its magnitude at low temperatures of around −30°C. It is noted that the M'' still retains its positive values at low temperatures at which M' exhibits negative values.

As in the case of the crystal-orientation dispersion of D_k^*, the anomalous dispersion behavior of M^* mentioned above must result from a composite-dispersion process and be treated in terms of multiple-dispersion mechanisms of orientational birefringences of different structural units with different intrinsic birefringences plus some distortional birefringence of interlamellar noncrystalline materials. The multiple optical-retardation processes may be analyzed through the apparent master curves of M^* by describing phenomenologically as follows.

$$M'_T(\omega)=\sum_{j=1}^{m} q_{T_j}(T,\ T_0)\left[M'_{j,T_0}(\infty)+\int_{-\infty}^{\infty} M_{j,T_0}(ln\tau)\frac{d ln\tau}{1+\omega^2\tau_j^2(T_0)o_{T_j}^2}\right]$$
$$=\sum_{j=1}^{m} q_{T_j}(T,\ T_0)[M'_{j,T_0}(\infty)+M'_{j,T_0}(\omega o_{T_j})] \tag{5}$$

$$M''_T(\omega)=\sum_{j=1}^{m} q_{T_j}(T,\ T_0)\times\left[\int_{-\infty}^{\infty} M_{j,T_0}(ln\tau)\frac{\omega\tau_j(T_0)o_{T_j}\,d ln\tau}{1+\omega^2\tau_j^2(T_0)o_{T_j}^2}\right]$$
$$=\sum_{j=1}^{m} q_{T_j}(T,\ T_0)[M''_{j,T_0}(\omega o_{T_j})] \tag{6}$$

where $M_j(ln\,\tau)$ is the stress-optical retardation spectrum of the jth optical-dispersion mechanism,[24] and q_{T_j} and o_{T_j} are the vertical- and horizontal-shift factors for the jth mechanism, respectively.

The apparent master curves of M' and M'' reduced to a reference tempearture of 50°C are depicted in Figure 24. These master curves are obtained by superposing horizontally the $q_T M'$ and $q_T M''$ for which compensation has been made by an amount of q_T prior to superposition so that no vertical translation is required in the superposition. It is seen that M' drastically decreases with increasing reduced frequency and reverses its sign

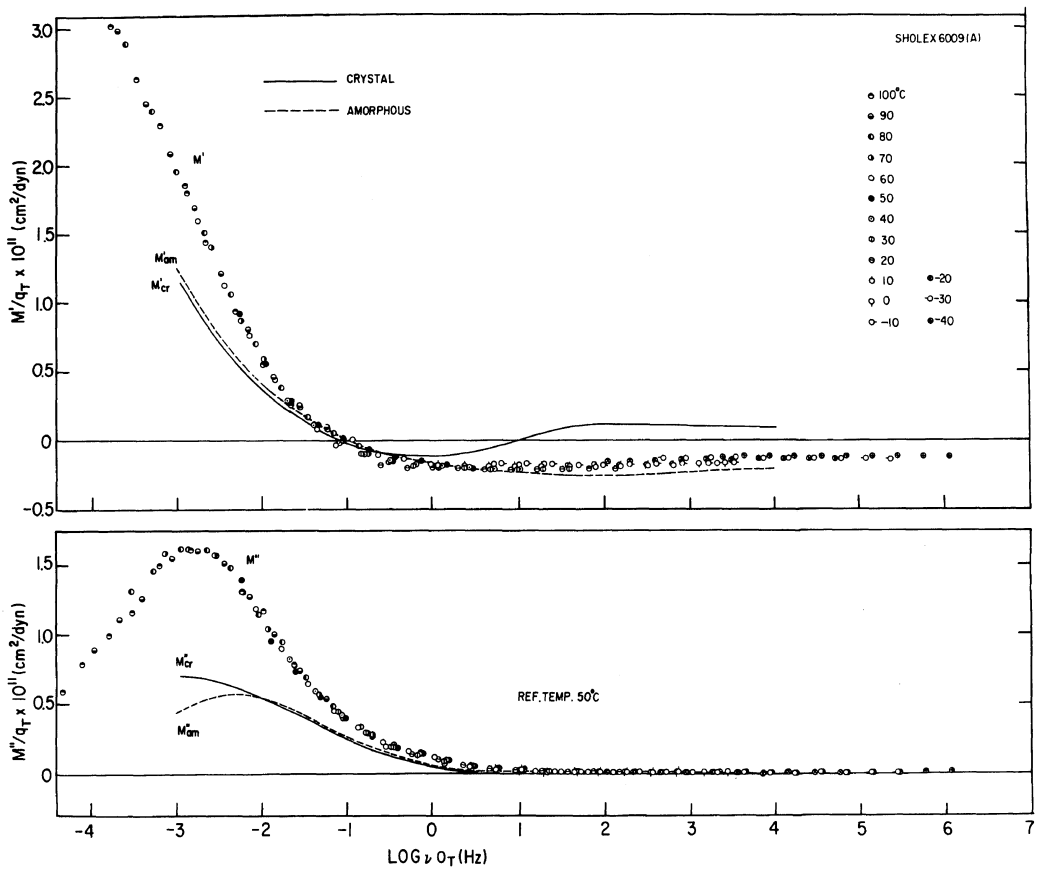

Figure 24. The superposed master curves of the real and imaginary components of the complex dynamic stress-optical coefficient function reduced to a reference temperature of 50°C in comparison with those of crystalline and noncrystalline contributions.

from positive to negative while exhibiting a shallow maximum with a negative sign in a frequency range around 10 Hz. M'' shows a distinct peak at low reduced frequencies around 10^{-3} Hz. M'' also decreases drastically with increasing reduced frequency, but continues to remain at positive values. The opposite signs of M' and M'' at high reduced frequencies in association with the appearance of a shallow negative maximum in M' suggest the existence of multiple-retardation processes in the optical dispersion, *i.e.*, the crystal-reorientation and lamellar-orientation processes. This was suggested in the previous section on dynamic crystal-orientation dispersion and will be discussed in detail later in connection with dynamic noncrystalline-orientation dispersion.

The apparent horizontal- and vertical-shift factors, o_T and q_T, are plotted as a function of temperature in Figures 25 and 26, respectively. Two linear regions appear in the Arrhenius plots of o_T from which the activation energies of the optical-retardation processes are estimated to be 17.2 and 24.2 kcal mol^{-1}, respectively. These values and their corresponding temperature regions suggest the occurrence of β and α birefringence dispersions. It is noteworthy that these activation energies are in good agreement with those of β and α crystal-orientation dispersions as well as with those of β and α_1 mechanical dispersions, respectively. It is of interest that no dispersion corresponding to the mechanical α_2 dispersion could be observed in either the birefringence nor the crystal-orientation

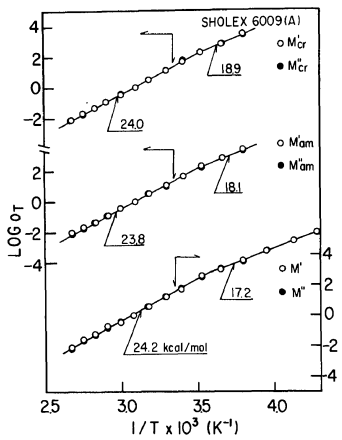

Figure 25. The Arrhenius plots of horizontal-shift factors log o_T *vs.* reciprocal absolute tempeature for the complex dynamic stress-optical coefficient function M^* comparing with those of crystalline and noncrystalline contributions, M^*_{cr} and M^*_{am}.

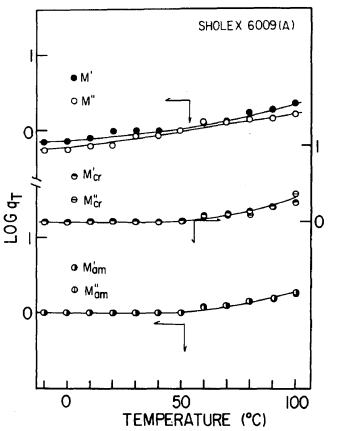

Figure 26. The temperature dependence of vartical-shift factors log q_T for M^* comparing with those of M^*_{cr} and M^*_{am}.

dispersions.

Juding from the activation energies and the temperature regions, the β birefriengence dispersion corresponds to the β crystal-orientation dispersion and further to the β mechanical dispersion, while the α birefringence dispersion corresponds to the α crystal-orientation dispersion covering the region from -40 up to room temperature. The negative birefringence mechanism of lamellar orientation (β crystal-orientation mechanism) associating with interlamellar noncrystalline orientation is known to prevail. Hence, the same mechanism may be expected to activate the β mechanical dispersion, though the problem of the opposite signs of M' and M'' in this region are left unsolved. The α birefringence dispersion is found to occur in the vicinity of the α_1 and α_2 mechanical dispersion regions covering a temperature range higher than room temperature where M' gradually changes its sign from negative to positive with increasing temperature or decreasing frequency. The predominant mechanism in the α birefringence dispersion region is the reorientation of the crystal grains within the orienting lamellae so as to align the crystal c-axis in the stretching direction. It should be, however, emphasized that the reorientation process can occur in the vicinity of α_2 mechanical dispersion region as well such that the activation energy may be the same as that in the vicinity of α_1 mechanical dispersion region.

The temperature dependence of the verical-shift factor q_T shown in Figure 26 is not easily explained. This is because q_T, being an apparent factor, is not simply related to q_{T_j} in eq 5 and 6. As recognized from the definition of M^* and q_{T_j}, q_T must be a complicated function of the temperature dependences of the intrinsic birefringence and mechanical compliance of the jth mechanism as well as the degree of crystallinity of the system.

DISCUSSION

The dynamic birefringence dispersion results from the contributions of both the crystalline and noncrystalline phases. The crystalline contribution can be quantified directly from the crystal-orientation dispersion investigated in the dynamic X-ray diffraction studies of the previous section. The noncrystalline contribution, though indirect, can be evaluated on the basis of a two-phase hypothesis by subtracting the crystalline contribution from the total birefringence. Accordingly, it is plausible to extend the discussion on the α and β birefringence dispersions quantitatively in terms of the contributions from both phases.

In general, the stress-optical coefficient function may be expressed for an uniaxially oriented polyethylene as follows.[42]

$$M=(\partial\Delta n/\partial\sigma)|_{\sigma=\sigma^0}=X_c[(n_a-n_c)D_a+(n_b-n_c)D_b]$$

$$+(1-X_c)\Delta^0_{am}D_{am}+(\partial\Delta_f/\partial\sigma)$$
$$=M_{cr}+M_{am}+M_f \quad (7)$$

where X_c is the volume fraction of crystalline phase, n_k is the principal refractive index of polyethylene crystal, D_k is the stress-orientation coefficient of the kth crystallographic axis or noncrystalline chain segment axis, and Δ^0_{am} is the intrinsic birefringence of noncrystalline chain segment. The subscripts cr, am, and f denote the crystalline, noncrystalline, and form birefringences, respectively.

For the complex dynamic stress-optical coefficient function, eq 7 may be modified by rewriting the M and D in terms of the complex variables as follows.

$$M^*_T(i\omega)=X_c\sum_k^{a,b}(n_k-n_c)_T D^*_{k,T}(i\omega)$$
$$+[1-X_c(T)]\Delta^0_{am}D^*_{am,T}(i\omega)+(\partial\Delta^*_f/\partial\sigma^*)$$
$$=M^*_{cr,T}(i\omega)+M^*_{am,T}(i\omega)+M^*_{f,T}(i\omega) \quad (8)$$

The last term in eq 8 is usually assumed to be negligibly small for spherulitic-crystalline specimens.* Hence, eq 8 may be reduced to

$$M^*_T(i\omega)=M^*_{cr,T}(i\omega)+M^*_{am,T}(i\omega) \quad (8')$$

The principal refractive indices of a polyethylene crystal are assumed to be the same as those of *n*-paraffin; *i.e.*, $n_a=1.514$, $n_b=1.519$, and $n_c=1.575$ as determined by Bunn and Daubeny.[43] These indices are further assumed to be temperature independent. The separation of crystalline and noncrystalline contributions from original birefringence dispersion data in Figures 22 and 23 can be carried out in accordance with eq 8′ by using the temperature dependence of $X_c(T)$ in Figure 3 as well as original data of D^*_k in Figures 10 and 11. The separated results for the crystalline and noncrystalline contributions, $M^*_{cr,T}(i\omega)$ and $M^*_{am,T}(i\omega)$, are plotted against frequency in Figures 27 and 28, respectively,

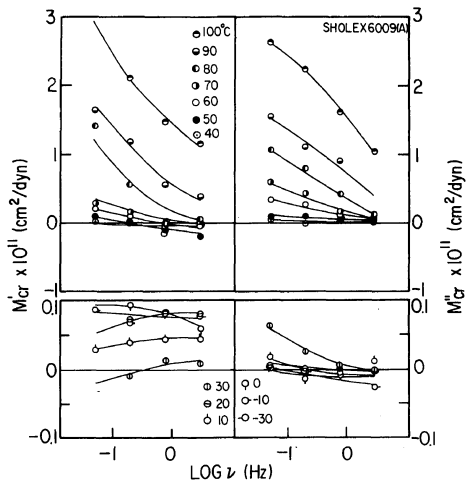

Figure 27. The variations in the real and imaginary components of crystalline contribution in the complex dynamic stress-optical coefficient function, M'_{cr} and M''_{cr}, with frequency in high- and low-temperature regions.

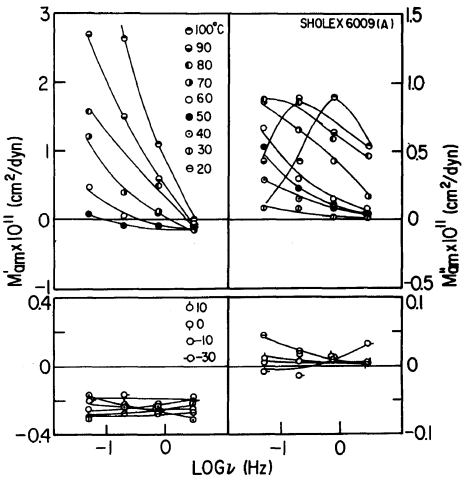

Figure 28. The variations in the real and imaginary components of noncrystalline contribution in the complex dynamic stress-optical coefficient function, M'_{am} and M''_{am}, with frequency at high- and low-temperature regions.

* Such an assumption has been widely practiced and found reasonable in the vicinity of the α birefringence dispersion even for the MD specimen of row-nucleated polyethylene[26,27] for which the orientational birefringence dispersion of crystal grains within crystal lamellae is greatly predominant over the form birefringence dispersion arising from dynamic orientation (splaying apart) of the crystal lamellae. However, caution should be exercised in ignoring the influence of form birefringence at low temperatures probably in the vicinity of β dispersion region. This is because the form birefringence may become comparable with the orientational birefringence of crystal lamellae at glassy temperatures even for spherulitic polyethylene, provided that the lamellar orientation (splaying apart mechanism) is concentrated at equatorial zone of the spherulites. Nevertheless for the moment, ignoring the form birefringence is for the purpose of simplicity, and the resulting shortcomings will be discussed later.

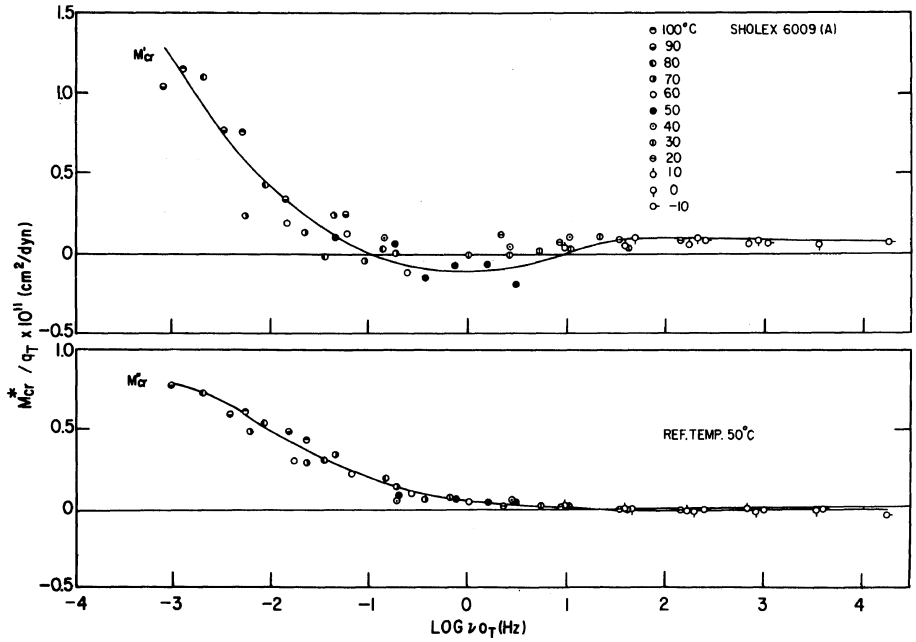

Figure 29. The superposed master curves of the real and imaginary components of crystalline contribution in the complex dynamic stress-optical coefficient function, reduced to a reference temperature of 50°C.

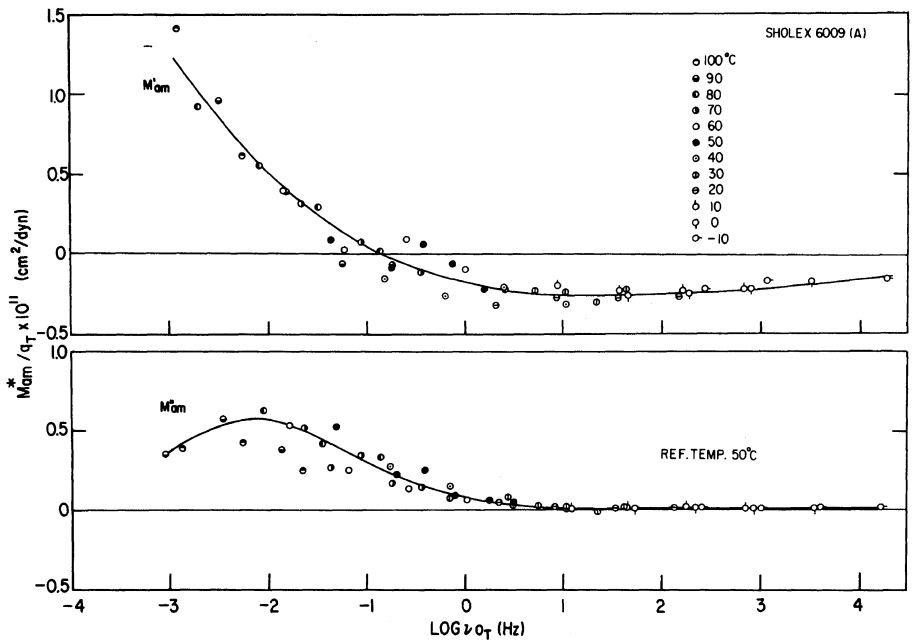

Figure 30. The superposed master curves of the real and imaginary components of noncrystalline contribution in the complex, dynamic stress-optical coefficient function, reduced to a reference temperature of 50°C.

by dividing into high- and low-temperature regions.

The frequency dependences of the real and imaginary components of complex dynamic stress-optical coefficient function of the crystalline phase, M^*_{cr} $(=M'_{cr}-iM''_{cr})$, resemble, in their behavior, those of the dynamic crystal *c*-axis orientation, D^*_c, in which the relative contributions of the lamellar-orientation and intralamellar crystal-reorientation processes are of crucial importance to account for the mechanisms of β and α orientation dispersions. The same mechanisms are expected to prevail in the β and α birefringence dispersions. However, as can be noticed from Figure 28, a substantial contribution from the amorphous phase can be realized from the frequency-dispersion behavior of M^*_{am}, suggesting that the crystal orientations are not the sole processes that prevail in the β and α birefringence dispersions. M'_{am} is positive at high temperatures, but reverses its sign to negative as temperature decreases, whereas M''_{am} is positive for all temperatures. This is undoubtedly at variance with the conventional interpretation in regard to the single optical-retardation process. That is, the noncrystalline contribution at relatively low temperatures must result not only from the orientational birefringence of noncrystalline chain segments but also from the form birefringence, as pointed out in the previous foot note, and possibly from the distortional birefringence of noncrystalline chains, whose relative contribution to M^*_{am} will be discussed qualitatively in later.

The frequency-temperature superposition is established for the M^*_{cr} and M^*_{am} separately, and is reduced to a common reference temperature of 50°C. A correction factor q_T is applied in both cases prior to the superposition, as was carried out for M^* previously. The master curves thus obtained for the crystalline and noncrystalline phases are shown in Figures 29 and 30, respectively. The M'_{cr} which is positive at high reduced frequencies, reverses its sign from positive to negative at moderate frequencies, and then changes to positive again as frequency decreases or temperature increases. M''_{cr} is slightly negative at high reduced frequencies, but reverses its sign to positive and increases profoundly with decreasing frequency. These frequency-dispersion behavior are exactly what were seen in the crystal *c*-axis orientation behavior in Figure 12 and schematized in Figure 14. It is therefore believed that the behavior of M^*_{cr} can possibly be explained on the basis of the relative contributions of the lamellar-orientation and intralamellar crystal-reorientation processes. Moreover, the Arrhenius plots of horizontal-shift factor for composing the master curves of M^*_{cr} *vs.* reciprocal absolute temperature consist of two straight lines from whose slopes the activation energies of the respective processes were estimated to be 24.0 and 18.9 kcal mol^{-1}, as shown in Figure 25.

The M'_{am} is negative at high reduced frequencies. It changes toward positive with decreasing frequency or increasing temperature. The corresponding M''_{am} is slightly positive but shows a distinct peak at low reduced frequencies. The activation energies as estimated from the Arrhenius plots of horizontal-shift factors *vs.* reciprocal absolute temperature are of the order of 23.8 and 18.1 kcal mol^{-1}, respectively, for the high- and low-temperature processes, as shown in Figure 25. These values certainly resemble those of the α and β processes obtained in the M^* and M^*_{cr}.

The master curves, of M^*, M^*_{cr} and M^*_{am} are compared in Figure 24. At the low frequency or high-temperature region, the $M'_{cr} \simeq M'_{am}$ and $M''_{cr} \simeq M''_{am}$, indicating that the phase angles of the crystalline and noncrystaline responses with respect to the bulk stress must be equal. This fact, in addition to the above identical activation energies for the α processes of M^*_{cr} and M^*_{am}, implies that the crystalline and noncrystalline orientations occur concurrently in the vicinity of the α dispersion. It is, therefore, believed that the responding noncrystalline phase in the α dispersion region must be the phase at the crystal grain boundary so that it responds almost in the same phase with the crystal-grain orientation. This is a distinctive evidence enabling one to assign the α_1 mechanical dispersion to the crystal grain boundary phenomena. Comparing the above well-correlated responses of the crystalline and noncrystalline phases for this spherulitic high-density polyethylene to the rather less associated responses for a spherulitic low-density polyethylene[22,24] both in the α dispersion region, the contrast seems to be related to the contradictory behavior in J^*_k between the specimens, as mentioned previously. However, a concrete explanation for this in terms of any morphological or topological aspect is still uncertain.

On the other hand, the behavior of M^*_{cr} and M^*_{am} at high and moderate frequencies are considerably

different. Although the behavior of M^*_{cr} at these reduced-frequency regions can be explained in terms of the prevalence of the lamellar-orientation process over the crystal grain orientation process, the interpretation of the M^*_{am} is by no means straightforward; *i.e.*, M'_{am} is considerably negative while M''_{am} is slightly positive. This can not be explained in terms of a single optical-retardation process, such as orientational birefringence of noncrystalline chain segments having positive intrinsic birefringence.

Let us assume that three different components contribute to the negative M'_{am} and slightly positve M''_{am}: *i.e.*, i) positive orientation of interlamellar noncrystalline materials, such as orientations of tie-chain molecules as well as end-to-end vectors of looped chain molecules both in association with lamellar orientation to give positive $M'_{am,ori}$ and positive $M''_{am,ori}$; ii) form birefringence owing to dynamic orientation of crystal lamellae at equatorial zone of uniaxially deformed spherulites, as pointed out in the previous footnote to give negative $M'_{am,f}$ and negative $M''_{am,f}$; iii) distortional birefringence due to distortions in the local structures of noncrystalline chains, such as bond stretching, valence angle distortion, etc. at glassy temperatures, giving $M'_{am,dis}$ and $M''_{am,dis}$. This results in

$$\begin{aligned} M'_{am} &= M'_{am,ori} + M'_{am,f} + M'_{am,dis} \\ M''_{am} &= M''_{am,ori} + M''_{am,f} + M''_{am,dis} \end{aligned} \tag{9}$$

In order to make M'_{am} considerably negative while M''_{am} slightly positive, $M^*_{am,dis}$ with a considerably negative $M'_{am,dis}$ and almost zero $M''_{am,dis}$ must be taken into account, at least qualitiatively.

At glassy temperatures, the contribution from distortional birefringence may be conceivable, as in the case of amorphous polymers. According to studies by Read, the distortional birefringence of polyacetaldehyde (PAC)[44] and poly(methyl acrylate) (PMA)[45] both contribute toward positve values below their glass-transition temperatures, *i.e.*, the real components of both strain-optical and stress-optical coefficients are positive at the glassy temperatures. The rise in temperature releases local distortion and produces an increase in the average orientation of chain links. This leads to an increase in birefringence in the case of PAC but to a decrease in birefringence toward negative values for PMA, depending on the nature of their intrinsic birefringence of the chain segments. The positive birefringence contribution due to distortion was also reported by Stein for lactoprene polymer[46] whose stress-optical coefficient below the glass-transition temperature was slightly positive but drastically decreased to large negative value as the temperature increased above T_g. The positive distortional birefringence is not always the case. According to Utsuo and Stein,[47] glassy poly(vinyl chloride) (PVC) has a small negative value due to distortional birefringence while rubbery PVC has a much larger positive value as a result of orientational birefringence.

At present, since there is no report on the distortional birefringence for polyethylene, it is uncertain whether the distortional birefringence contributes toward positive or negative values. Also, it is rather hard to predict whether the distortional birefringence is time-dependent or not, *i.e.*, $M''_{am,dis}$ being zero or finite, in the frequency and temperature ranges of the present experiment. If the distortional birefringence contribution in polyethylene is negative in sign and has a time-independent nature, such a contribution may be of crucial importance to account for the negative M'_{am} with slightly positive M''_{am}. One of recommended means for dealing with this complex behavior in the noncrystalline phase may be dynamic infrared dichroism by which it should be possible to follow the responses of specific noncrystalline bands.

CONCLUSION

The deformation mechanisms underlying the α and β mechanical dispersions of a spherulitic high-density polyethylene were explored by means of dynamic birefringence and dynamic X-ray diffraction techniques. Three mechanical dispersions analogous to the β, α_1 and α_2 processes were observed and resolved into each component, quantitatively. Two dispersions corresponding to α and β processes were detected in the dynamic crystal-orientation studies. These α and β orientation dispersion processes were interpreted in terms of the relative contributions of the intralamellar crystal grain orientation and lamellar orientation, both associated with dynamic tensile deformation of the spherulitic-crystalline texture. In the dynamic crystal-lattice deformation studies, two dispersions corresponding to the α_1 and α_2 mechanical dispersions were observed. The former α_1 lattice disper-

sion is considered to be associated with the α crystal orientation dispersion, whereas the latter α_2 lattice dispersion is believed to be inherent, arising from the incoherent lattice vibrations within crystals in which the intermolecular potential suffers a smearing out effect.

In complementary studies on dynamic birefringence, only α and β dispersion processes, analogous to the α and β crystal orientation dispersion processes, where obtained. The crystalline and noncrystalline contributions to the birefringence dispersions were separated on the basis of a two-phase hypothesis. Besides the α crystal-orientation contribution, a substantial noncrystalline contribution was seen and is believed to result from the orientation of noncrystalline chains at the crystal grain boundaries. The noncrystalline contribution to the β dispersion process was observed with a large negative in-phase component and a slightly positive out-of-phase component of the stress-optical coefficient function. This anomalous behavior may be explained in terms of combined contributions from orientational and distortional birefringences of interlamellar noncrystalline chains as well as from negative form birefringence.

Finally, it is concluded that (i) the β mechanical dispersion of a spherulitic high-density polyethylene is a process of dynamic lamellar orientation associated with the orientation and distortion of interlamellar noncrystalline chains, (ii) the α_1 mechanical dispersion is a process of intralamellar crystal grain orientation associated with orientation of noncrystalline chains at the crystal grain boundaries, and (iii) the α_2 mechanical dispersion is a process of crystal-lattice dispersion associated with a smearing-out effect of intermolecular potential within crystal.

Acknowledgements. This series of rheo-optical studies on the deformation mechanism of semicrystalline polymers has been supported in part by a grant from the U.S.-Japan Cooperative Research Program of the National Science Foundation and the Japan Society for Promotion of Science. The authors are also indebted to the Nippon Gosei Kagaku Co., Ltd., Osaka, Japan and the Dai-Cell Chemical Industries Ltd., Osaka, Japan, for financial support through a scientific grant.

REFERENCES

1. J. D. Ferry, "Viscoelastic Properties of Polymers," Wiley, New York, N.Y., 1961.
2. N. G. McCrum, B. E. Read, and G. Williams, "Anelastic and Dielectric Effects in Polymeric Solids," Wiley, New York, N.Y., 1967.
3. N. Saito, K. Okano, S. Iwayanagi, and T. Hideshima, in "Solid State Physics," H. Ehrenreich, F. Seitz, and D. Turnbull, Ed., Vol. 14, Academic Press, New York, N. Y., 1963, p. 458.
4. S. Iwayanagi and H. Nakane, *Rep. Prog. Polym. Phys. Jpn.*, **7**, 179 (1964); Abstract, 5th International Congress on Rheology, Kyoto, 1968, p 40.
5. N. G. McCrum and E. L. Morris, *Proc. R. Soc. London, Ser. A*, **292**, 506 (1966).
6. H. Nakayasu, H. Markovitz, and D. J. Plazek, *Trans. Soc. Rheol.*, **5**, 261 (1961).
7. K. H. Sinnott, *J. Appl. Phys.*, **37**, 3385 (1966); *J. Polym. Sci., C*, **14**, 141 (1966).
8. M. Takayanagi and T. Matsuo, *J. Macromol. Sci., Phys.*, **B1**, 407 (1967).
9. J. D. Hoffman, G. Williams, and E. Passglia, *J. Polym. Sci., C*, **14**, 173 (1966).
10. Z. H. Stachurski and I. M. Ward, *J. Macromol. Sci., Phys.*, **B3**, 445 (1969).
11. T. Hideshima and M. Kakizaki, *J. Macromol. Sci., Phys.*, **B8**, 368 (1973).
12. T. Kajiyama, T. Okada, and M. Takayanagi, *J. Macromol. Sci., Phys.*, **B9**, 391 (1974).
13. T. Kajiyama, T. Okada, A. Sakoda, and M. Takayanagi, *J. Macromol. Sci., Phys.*, **B7**, 583 (1973).
14. K. Inohara, K. Imada, and M. Takayanagi, *Polym. J.*, **4**, 232 (1973).
15. S. Iwayanagi and I. Miura, *J. Appl. Phys. Jpn.*, **4**, 94 (1965).
16. A. Peterlin and E. W. Fischer, *Z. Phys.*, **159**, 272 (1961).
17. A. Peterlin, E. W. Fischer, and Chr. Reinhold, *J. Chem. Phys.*, **37**, 1403 (1962).
18. K. Okano, *Rep. Inst. Phys. Chem. Res.*, **40**, 295 (1964).
19. K. Okano, *J. Polym. Sci., C*, **15**, 95 (1966).
20. R. Hayakawa and Y. Wada, *Rep. Prog. Polym. Phys. Jpn.*, **11**, 215 (1968).
21. Y. Wada and R. Hayakawa in "Progress in Polymer Science, Japan," Vol. 3, S. Okamura and M. Takayanagi Ed., Kodansha, Tokyo, 1972, p 215.
22. S. Suehiro, T. Yamada, H. Inagaki, T. Kyu, S. Nomura, and H. Kawai, *J. Polym. Sci., Polym. Phys. Ed.*, **17**, 763 (1979).
23. S. Suehiro, T. Kyu, K. Fujita, and H. Kawai, *Polym. J.*, **11**, 339 (1979).
24. T. Kyu, S. Suehiro, S. Nomura, and H. Kawai, *J. Polym. Sci., Polym. Phys. Ed.*, in press.

25. S. Suehiro, T. Yamada, T. Kyu, K. Fujita, T. Hashimoto, and H. Kawai, *Polym. Eng. Sci.*, **19**, 929 (1979).
26. T. Kyu, N. Yasuda, S. Suehiro, T. Hashimoto, and H. Kawai, *Polymer,* in press.
27. T. Kyu, S. Suehiro, and H. Kawai, *Polym. J.*, **12**, 251 (1980).
28. T. Kyu, N. Yasuda, M. Tabushi, S. Nomura, and H. Kawai, *Polym. J.*, **7**, 108 (1975).
29. S. Suehiro, T. Yamada, H. Inagaki, and H. Kawai, *Polym. J.*, **10**, 315 (1978).
30. T. Oda, S. Nomura, and H. Kawai, *J. Polym. Sci., A*, **3**, 1993 (1965).
31. T. Oda, N. Sakaguchi, and H. Kawai, *J. Polym. Sci., C*, **15**, 223 (1966).
32. S. Nomura, A. Asanuma, S. Suehiro, and H. Kawai, *J. Polym. Sci., A-2,* **9**, 1991 (1971).
33. S. Nomura, M. Matsuo, and H. Kawai, *J. Polym. Sci., Polym. Phys. Ed.*, **10**, 2489 (1972).
34. S. Nomura, M. Matsuo, and H. Kawai, *J. Polym. Sci., Polym. Phys. Ed.*, **12**, 1371 (1974).
35. M. Nakatani, K. Iijima, S. Suganuma, and H. Kawai, *J. Macromol. Sci., Phys.*, **B2**, 55 (1968).
36. K. Tajiri, Y. Fujii, M. Aida, and H. Kawai, *J. Macromol. Sci., Phys.*, **B4**, 1 (1975).
37. Z. W. Wilchinsky, *J. Appl. Phys.*, **30**, 792 (1959).
38. H. Kawai, T. Hashimoto, S. Suehiro, and T. Kyu, to be presented at the 8th International Congress on Rheology, Naples, Italy, 1980.
39. R. J. Cembrola, T. Kyu, R. S. Stein, S. Suehiro, and H. Kawai, paper presented at the 2nd General Meeting of the American Physical Society, New York, N.Y., March 24—28, 1980; submitted to *J. Polym. Sci., Polym. Phys. Ed.*
40. H. Niwa, K. Fujita, T. Kyu, and H. Kawai, in preparation.
41. R. J. Cembrola, T. Kyu, S. Suehiro, H. Kawai, and R. S. Stein, paper presented at the 178th National Meeting of the American Chemical Society, Washington, September 9—14, 1979; to be submitted to *J. Polym. Sci., Polym. Phys. Ed.*
42. R. S. Stein, T. Kawaguchi, I. Kimura, and A. Takeuchi, *J. Polym. Sci., B*, **5**, 339 (1967).
43. C. W. Bunn and R. Daubeny, *Trans. Faraday Soc.*, **50**, 1173 (1954).
44. B. E. Read, *J. Polym. Sci., C*, **5**, 87 (1963).
45. B. E. Read, *Polymer,* **5**, 1 (1964).
46. R. S. Stein, in "Der Physik der Hochpolymeren," Vol. IV, H. A. Stuart, Ed., Springer, Berlin, 1956.
47. A. Utsuo and R. S. Stein, *J. Polym. Sci., A-2*, **5**, 583 (1967).